NANO LETTERS

2008
Vol. 8, No. 3
962-967

Measuring the Redox Activity of Individual Catalytic Nanoparticles in Cerium-Based Oxides

Ruigang Wang,*,† Peter A. Crozier,* Renu Sharma, and James B. Adams

LeRoy Eyring Center for Solid State Science, School of Materials, Arizona State University, Tempe, Arizona 85287-1704

Received December 1, 2007; Revised Manuscript Received January 14, 2008

ABSTRACT

We have followed the dynamic redox process taking place in individual ceria zirconia nanoparticles with changes in the oxygen chemical potential using an in situ environmental transmission electron microscopy (ETEM). We observe considerable variability in the redox activity and have been able to correlate these differences with nanoscale structural and compositional measurements. We find that the more active structure has predominantly disordered cations and shows no evidence for oxygen vacancy ordering during reduction.

Introduction. Nanoscale ceria zirconia particles are a critical component in the modern automotive three-way catalytic converter[1–4] and have potential applications in other areas such as fuel cells where redox functionality is important.[5,6] The catalytic action is associated with the ability of Ce to easily switch its oxidation state with changes in the oxygen chemical potential. An ongoing challenge for many catalysts is the difficulty associated with correlating catalytic activity with underlying nanoparticle parameters such as particle size, shape, structure, composition, and surface structure. Most methods of characterizing catalyst activity determine the average properties of the entire ensemble of particles. This is a vital step in identifying useful catalyst formulations, but it averages over the rich nanoscale variations that must be explored if a deep understanding of the structure–property relations is to be elucidated. This limitation is particularly important in many reducible oxide catalysts where subtle and dynamic variations in nanoparticle structure and stoichiometry under reducing conditions may play a vital role in catalytic functionality. For example, partially reduced cerium oxide is unstable at low temperatures and/or in high oxygen partial pressure and must be characterized in situ under strong reducing atmospheres. Moreover, under reaction conditions, the active components of the catalyst may not be static and may continually undergo phase transformations as a result of variations in temperature, gas composition, and pressure. For example, in the ceria zirconia system, the prior redox history of a particular sample strongly influences the overall low temperature reducibility of the material.[7–12]

Here we demonstrate that in situ environmental transmission electron microscopy (ETEM) can be used to explore the dynamic interplay between ambient conditions, catalytic activity, and nanoparticle structure for the ceria zirconia system. By varying the oxygen chemical potential in the microscope, we can measure the redox activity of individual nanoparticles. Moreover, using a combination of in situ nanospectroscopy and imaging, we are able to correlate nanoscale changes in activity with nanoscale variations in composition and structure.

Experimental Section. High surface area samples of $50\%CeO_2 50\%ZrO_2$ samples were prepared by a spray freezing method.[7] Samples were calcined at 500 °C for 5 h in air and then subjected to three redox cycles (for each redox cycle: the sample was reduced in H_2 at 1000 °C for 2.75 h and subsequently reoxidized in air). Macroscopic reduction properties were characterized by thermogravimetric analysis (TGA) in a reducing atmosphere using a Setaram TG92 system. In situ nanocharacterization was performed in a reducing atmosphere of an ETEM Tecnai F20, operated at 200 kV and equipped with a Gatan imaging filter (GIF) and annular dark-field (ADF) detector. Ceria zirconia powder was dispersed over Pt grids and loaded into the microscope in a Gatan heating holder. The samples were heated progressively up to 600 °C in 1.5 Torr of dry H_2. Redox cycling was performed by raising and lowering the sample temperature while maintaining the same H_2 rich atmosphere. (Reoxidation may occur rapidly at temperatures below 600 °C due to residual background oxygen/water vapor in the sample area or in the ETEM column.) Time and temperature resolved high resolution electron microscopy (HREM) and electron energy loss spectra (EELS) were recorded to follow the

* Corresponding authors. E-mail: rgwang@lbl.gov (R.W.); crozier@asu.edu (P.A.C.). Telephone: 510-486-5573 (R.W.); 480-965-2934 (P.A.C.). Fax: 510-486-4881 (R.W.); 480-965-9004.

† Present address: Materials Sciences Division, Lawrence Berkeley National Lab, Berkeley, CA, 94720.

10.1021/nl073135c CCC: $40.75
Published on Web 02/06/2008

structural and chemical changes during the reduction and reoxidation. Nanoparticle activity was determined by measuring the changes in the Ce oxidation state from EELS data during heating and cooling. The change in the relative height of the peaks at the beginning of Ce $M_{4,5}$ edge in the energy loss spectrum is representative of a transformation of the Ce oxidation state from +4 to +3, i.e., M_5 is higher than M_4 for a +3 oxidation state and M_5 is lower than M_4 for a +4 oxidation state. Moreover, the Ce M_5/M_4 integrated peak intensity ratios can be used to quantitatively determine the Ce oxidation state.[13] We use this approach to follow the change in the Ce oxidation state of individual nanoparticles during in situ redox cycling of the material. We used the Zr $M_{4,5}$ edge at 180 eV and $CeM_{4,5}$ at 883 and 901 eV signals to determine the Ce/Zr atomic concentration ratio.[7] The ionization cross section for the Ce $M_{4,5}$ edge is not well-known, so instead we used an empirical approach to determine the appropriate cross-section ratio for quantification of the Ce/Zr concentration ratio.[7]

Macroscopic Reduction Properties. Figure 1a shows the mass loss profiles in 5%H_2/95%He obtained for samples during first (sample A), second (sample B), and third (sample C) TGA reduction. After each reduction, the sample was cooled to room temperature and exposed to air for reoxidation. In the cleaning pretreatment step, the first mass loss between 20 and 300 °C is attributed to the release of loosely bound adsorbates (such as water). There is no evident mass change during isothermal holding at 150 °C for all samples. Much larger mass loss was observed for the sample A, as it is the fresh, as-synthesized powder containing water and precursor residue. Samples A, B, and C show a little further mass loss during isothermal holding at 300 °C. All samples show a small mass gain during cooling from 300 to 150 °C.

After the cleaning pretreatment, we attribute further mass loss to reduction of Ce^{4+} to Ce^{3+} (accompanied by removal of lattice oxygen) during heating between 150 and 1000 °C (including the holding time at 1000 °C). If we assume that all the Ce is in the +4 oxidation state at the beginning of each TGA run at 300 °C, we can calculate the maximum mass change (due to oxygen loss) that should occur during heating in H_2 if all the Ce reduces to the +3 oxidation state. The determined reduction percentage during the TGA reduction processes were 100, 90, and 57% for samples A, B, and C, respectively. This result shows that the material progressively loses 10−30% of its "reducibility or activity" after each high temperature redox cycle even though the particle size only increased slightly (32 nm after the first redox, 38 nm after the second redox, and 39 nm after third redox, as determined by TEM and X-ray diffraction) and no significant particle morphology change is observed, as shown in Figure 2. Figure 1b shows the reduction temperature for these three samples according to differential analysis of mass loss curves in Figure 1a from 150 to 1000 °C. These reduction mass losses were centered at 486, 448, and 431 °C for sample A, B and C, respectively, showing a decrease in the reduction temperature after each redox cycle. Table 1summarizes the reduction percentage and temperature for

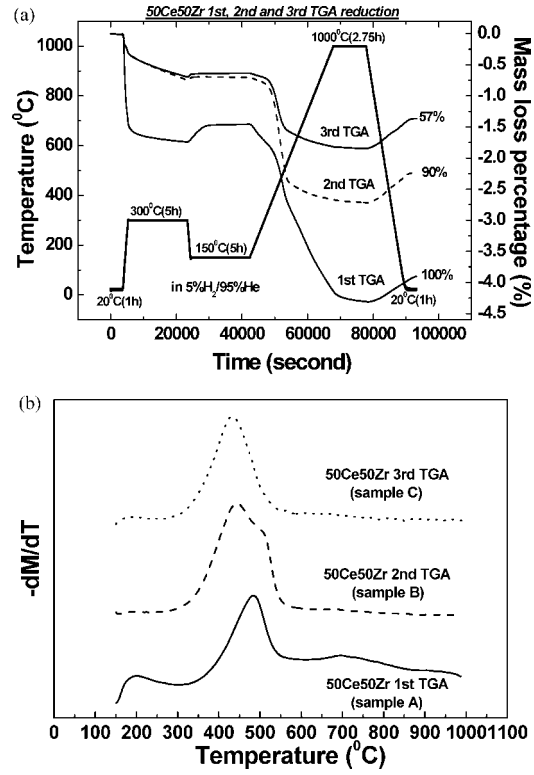

Figure 1. Mass loss (a) and corresponding derivative thermogravimetric profiles (b) showing the effect of high temperature redox cycling treatment on the reducibility. The reduction percentage is listed at the end of mass loss profile in (a).

the samples during first, second, and third TGA reduction. During the room temperature reoxidation in air after each reduction treatment, the color of the samples did not change back to the original yellow and became progressively darker after each redox cycle, suggesting incomplete reoxidation.

It has been reported that, for mixed ceria zirconia oxide samples subjected to "a severe reduction (5 h in H_2 at 950°C)" pretreatments, the average reduction temperature is lowered by 150 °C, resulting in improved oxygen storage capacity at low temperature.[1,14] Our TGA reduction measurements indicate that some component of the nanopowder is activated during the redox cycling, giving rise to a lowered reduction temperature, while another component of the material loses its activity, resulting in a decreased reduction percentage. This suggests that some form of heterogeneity is introduced to the powder during redox cycling, but there is no detectable phase transformation in these high surface area samples from XRD analysis after each redox cycle. These observations imply that subtle nanoscale structure and chemical changes within individual nanoparticles might be the key to understanding the origin of low temperature reduction and reduced reduction percentage.

Direct Activity Determination of Individual Nanoparticles. A series of in situ ETEM measurements on the sample after the first TGA reduction (sample A) was undertaken to explore the relationship between chemistry, structure, and redox activity of individual nanoparticles. The nanostructural and nanochemical changes that take

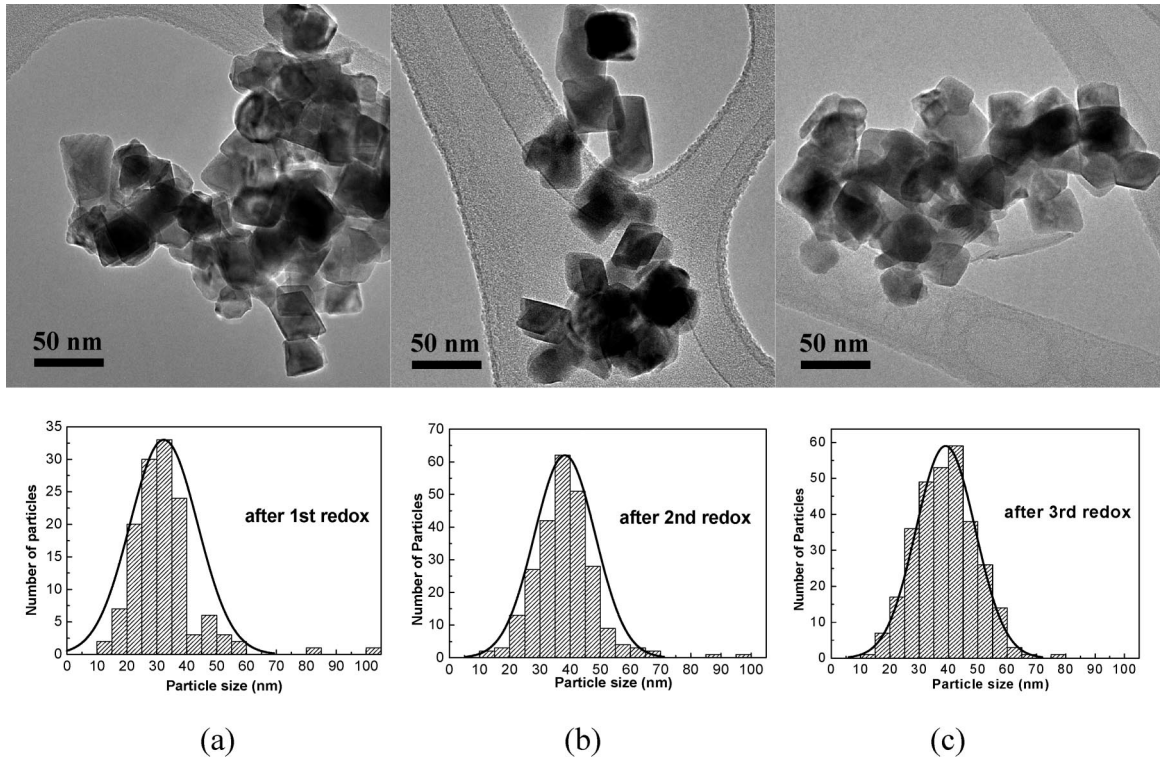

Figure 2. Particle morphology and size distribution of the samples after (a) 1st, (b) 2nd, and (c) 3rd redox cycling.

Table 1. Reduction Percentage and Temperature for 50%CeO_2 50%ZrO_2 Samples during Reduction

composition	sample notation	reduction percentage, %	reduction temperature °C
50%$CeO_2$50%ZrO_2	A (1st redox)	100	486
	B (2nd redox)	90	448
	C (3rd redox)	57	431

place in ceria zirconia during redox cycles were recorded in the ETEM with a constant H_2 flow. Parts a and b of Figure 3 show in situ HREM images and associated EELS spectra from two typical nominally identical nanoparticles (~20 nm) recorded at 580 °C in 1.5 Torr dry H_2, respectively. It is clear from the Ce white lines (insets) that there is a significant difference in the effect of the H_2 reducing environment on the oxidation state of these two nanoparticles. Analysis of Ce $M_{4,5}$ white line intensity ratio, obtained from EELS data, indicates that one particle (Figure 3b) is more strongly reduced than the other (Figure 3a). Figure 3c shows the variation in the oxidation state as a function of temperature over the range of 480−590 °C. A comparison of reduction behavior of these two particles as a function of temperature confirms the higher activity in one particle because its oxidation state changed from +4 to +3, while negligible change was observed for the other (Figure 3c), which means it was stable and relatively inactive. We note that the reduction temperatures in the ETEM are about 100 °C higher than those recorded during TGA. This is mainly caused by the much lower H_2 pressure present in the ETEM, which effectively increases the oxygen chemical potential.

The corresponding in situ EELS line scan profiles (not shown) across those same two nanoparticles were used to determine their average composition and compositional variation. From these EELS analysis, the active nanoparticle shows a lower Ce/Zr atomic ratio and stronger compositional variation within the grain. The average Ce composition for the active nanoparticle is 36%, whereas the inactive nanoparticle is 55%.

By heating and cooling in H_2, we followed the redox properties of 11 different nanoparticles of sample A shown in Table 2 and identified three distinct behaviors, which we label I, II, and III (see Figure 4a−c). Type I nanoparticles are the most active, and they reduce to close to the +3 oxidation state at approximately 590 °C and are reoxidized back their original oxidation state when cooled below 500 °C. Type II nanoparticles are significantly less active; although the temperature was kept at almost 590 °C for 1 h, the Ce reduced only to an average oxidation state of 3.5 and did not reoxidize when the sample was cooled to 480 °C. Type III nanoparticles reduced to almost the +3 oxidation state if held at about 590 °C for 1 h but did not reoxidize back to original oxidation state when cooled.

In situ identification of different redox behaviors in individual nanoparticles can explain the decreased reduction percentages determined by TGA analysis. The decreased oxygen loss associated with the relatively small oxidation state change in the less active nanoparticles (types II and III) will give rise to the decrease in the reduction percentages observed in TGA. Although the statistics of the ETEM measurements are somewhat limited, we can convert the redox measurements on individual nanoparticles (of known size) into an equivalent volume averaged reduction fraction to compare with the macroscopic TGA measurements. We assumed that the volume of each particle is proportional to

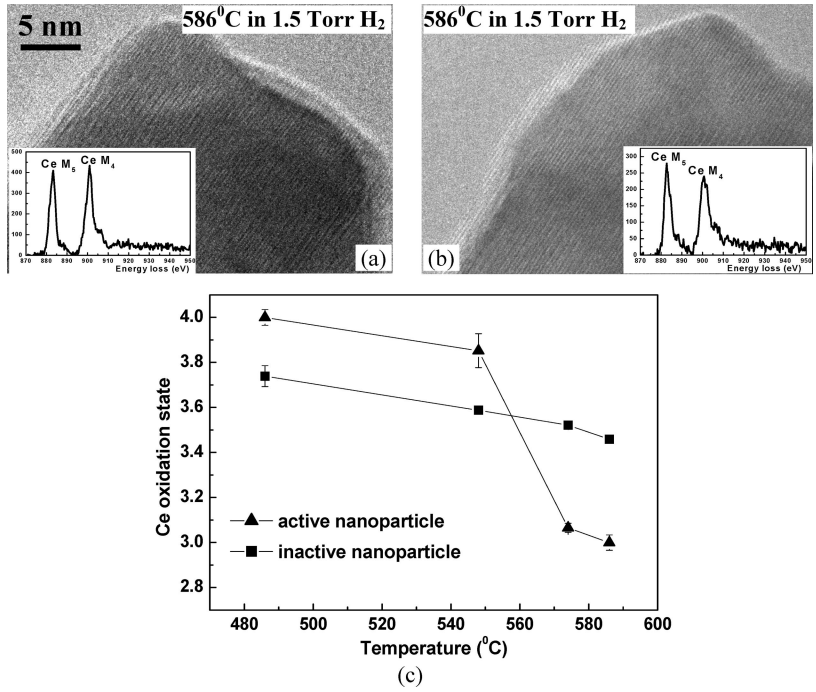

Figure 3. In situ HREM images (a) and (b) from nominally identical ceria zirconia nanoparticles recorded at 586 °C in 1.5 Torr of H_2. The in situ EELS (inserts) show that the particle on the right is more strongly reduced than the particle on the left. (c) Oxidation state for same two particles as a function of temperature.

Table 2. Ce Oxidation State Determined by Ce $M_{4,5}$ EELS during Redox Processes from 11 Individual Ceria Zirconia Nanoparticles (I, II, III Indicate Three Types of Redox Behavior of Particles Defined in the Text)

	Ce oxidation state				
	heating 480 °C	590 °C	cooling 470 °C	particle size (nm)	Ce composition (Ce/(Ce + Zr))
particle 1 (I)	3.5 ± 0.2	3.0 ± 0.1	3.5 ± 0.1	13.0	0.49 ± 0.09
particle 2 (I)	3.7 ± 0.2	3.1 ± 0.2	3.7 ± 0.2	14.3	0.48 ± 0.08
particle 3 (I)	3.7 ± 0.1	3.3 ± 0.1	3.6 ± 0.0	31.2	
particle 4 (II)	3.7 ± 0.2	3.5 ± 0.2	3.5 ± 0.1	20.0	0.55 ± 0.08
particle 5 (II)	3.7 ± 0.0	3.2 ± 0.1	3.4 ± 0.3	19.8	0.45 ± 0.06
particle 6 (II)	3.8 ± 0.1	3.2 ± 0.2	3.5 ± 0.1	15.6	0.46 ± 0.05
particle 7 (II)	3.8 ± 0.2	3.1 ± 0.2	3.4 ± 0.0	41.8	0.49 ± 0.05
particle 8 (II)	3.8 ± 0.3	3.2 ± 0.0	3.5 ± 0.2	9.0	0.42 ± 0.06
particle 9 (III)	4.0 ± 0.1	3.0 ± 0.1	3.8 ± 0.1	19.0	0.36 ± 0.07
particle 10 (III)	3.8 ± 0.2	3.1 ± 0.2	3.7 ± 0.2	33.7	0.49 ± 0.09
particle 11 (III)	3.9 ± 0.3	3.3 ± 0.1	3.8 ± 0.1	29.6	0.55 ± 0.10

the cube of the particles diameter. The volume weighted average Ce oxidation state of these 11 nanoparticles are 3.8, 3.2, and 3.6 at 480 °C (during heating up), 590 °C (highest temperature), and 470 °C (during cooling down), respectively. The final value of 3.6 is about 25% lower than the starting value of 3.8 so that in a subsequent redox cycle the volume of material available for reduction will be about 25% less. Given the limited statistics, this is reasonably consistent with the TGA measurement, which showed that about 10% of the material lost activity and showed no mass loss after the first high temperature redox cycle (see Table 1). Moreover, the TEM samples may reoxidize further when they are cooled from 470 °C to room temperature and exposed to air, which will increase the agreement between the two approaches.

Structure−Composition−Activity Relations. Although X-ray diffraction characterization shows the ceria zirconia solid solution nanopowders are single-phase (homogeneous), there is compositional and structural variation between nanoparticles at the nanoscale level, even within individual nanoparticles.[7] Now that we can determine the activity of the particles, we can use atomic resolution imaging and nanospectroscopy techniques available in the ETEM to explore the relationship between structure, composition, and activity for individual nanoparticles. A simple measure of the reducibility or reduction activity can be obtained from the change in Ce oxidation states during heating in H_2. We can define a particle reduction activity as

$$\text{activity} = \frac{\text{Ce}^x_{\text{initial}} - \text{Ce}^y_{\text{final}}}{\text{Ce}^x_{\text{initial}} - 3}$$

where $\text{Ce}_{\text{initial}}{}^x$ and $\text{Ce}_{\text{final}}{}^y$ represent the Ce oxidation state at 480 and 590 °C, respectively, and 3 is the lowest oxidation state of Ce. Figure 5 plots the reduction activity of 11 nanoparticles as a function of Ce concentration and shows the reduction activity decreases with Ce concentration in the

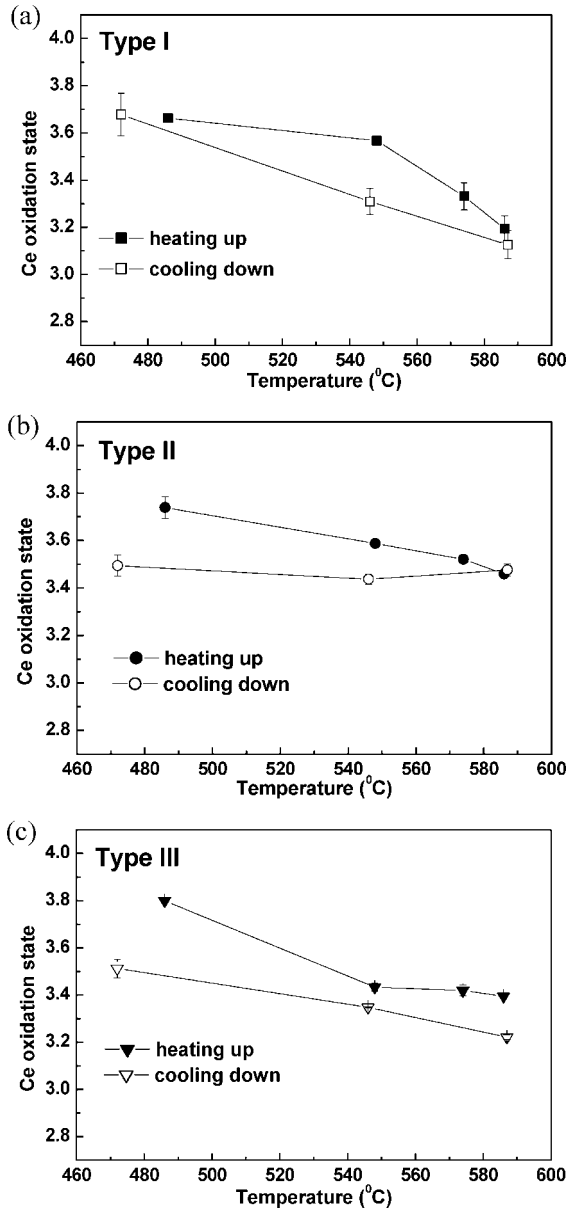

Figure 4. Three different types of redox behavior determined by EELS analysis from individual ceria zirconia nanoparticles during redox processes: (a) active nanoparticle, (b) inactive nanoparticle, and (c) initially active but not recyclable.

range of 36–55%. The most active particle has the lowest Ce concentration, but the particles close to 50% Ce also show excellent activity. This is consistent with ex situ bulk characterization, suggesting that 50Ce50Zr has optimal oxygen storage capacity.[14–16] It is clear that the redox activity of individual nanoparticles is influenced by particle composition. However, it is also apparent from Figure 5 that there can be substantial variations in the reduction activity among nanoparticles with similar composition, suggesting that structural changes may also play an important role. Atomic resolution imaging has also been used to reveal the structure of the particle, surface, and defect, allowing a complete description of particle nanostructure. Parts a and b of Figure 6 show high resolution images and related diffractograms for two typical structures found in sample A. Image simulations and diffraction analysis show that Figure 6a is consistent with the cubic fluorite-like structure that predomi-

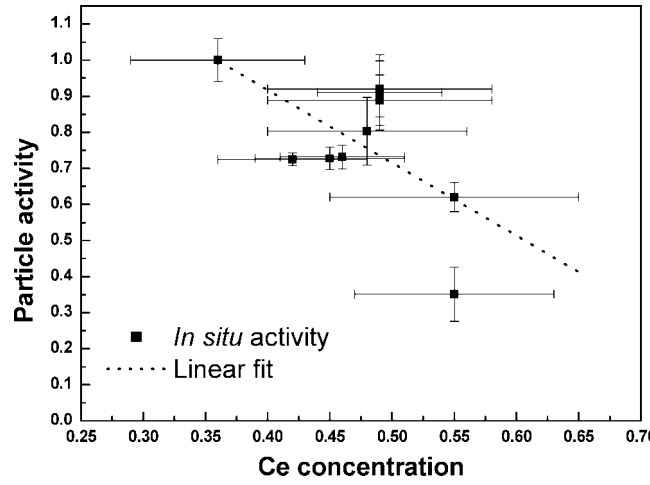

Figure 5. Reduction activity measurements of individual ceria zirconia nanoparticles during in situ reduction.

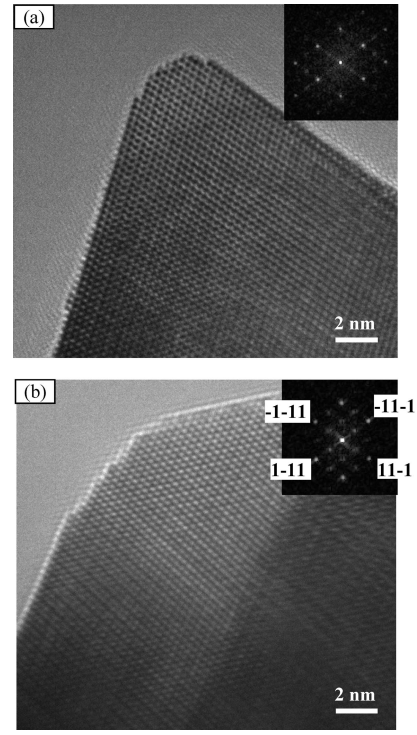

Figure 6. Nanoparticles with fluorite-like structure (a) and local cation-ordered pyrochlore superstructure (b) along [011] zone axis.

nates in these materials. These nanoparticles with cubic fluorite-like structure can be reduced to the +3 oxidation state and then reoxidized during in situ heating and cooling. They correspond to the active nanoparticles defined above. Moreover, we see no evidence for oxygen vacancy order during redox cycling.

The diffractogram and high resolution image of Figure 6b shows the presence of a superstructure in the ⟨111⟩ directions, which suggests a cation-ordered pyrochlore structure. HREM images and electron diffraction patterns were simulated to test this hypothesis, and they were found to be in good agreement with the experimental data. EELS analysis showed that Ce was in the +3 oxidation state for nanoparticles showing the superstructure, which is consistent with the

superstructure being the pure pyrochlore $Ce_2Zr_2O_7$ phase. Our observations are in agreement with earlier reports of cation ordering in ceria zirconia samples after high temperature redox cycling evidenced by Raman spectroscopy[11] and transmission electron microscopy (TEM) characterization.[15,16]

In pure pyrochlore, the oxidation state of Ce is already +3, so it is completely inactive during heating in hydrogen. Partially reoxidized pyrochlore-related phases, $Ce_2Zr_2O_{7+x}$ ($0 < x < 1$), can only be partially reduced. Compared with $Ce_2Zr_2O_8$ (or $CeZrO_4$ solid solution), the relative mass loss phases, $Ce_2Zr_2O_{7+x}$ ($0 < x < 1$), during reduction is smaller, assuming both of them can be completely reduced. The formation of those oxygen-deficient phases after high temperature reduction treatments are a major contributor to the decreased reduction percentage measured with both TGA and ETEM. Also the difference in reduction activity of the nanoparticles with 36% and 55% Ce (Figure 3c) may be because it is not possible to form these inactive cation-ordered pyrochlore phases for the nanoparticle with 36% Ce (in the $Ce_2Zr_2O_{7+x}$ pyrochlore-related phase, the required ratio of Ce/Zr is 1).

In summary, we have demonstrated that ETEM can allow us to detect variations in redox behavior of individual nanoparticles. This provides us with an exciting opportunity to isolate and identify the phases with different redox activity in catalytic nanoparticles of cerium-based oxides. Our nanometer measurements of reducibility are in reasonable agreement with the result of macroscopic measurement such as TGA. We have been able to correlate the activity of individual nanoparticles with both nanochemistry and nanostructure. We find that the reduction activity of individual nanoparticles decreases with Ce concentration in the range of 36–55% Ce. The most active particle has the lowest Ce concentration and a predominant fluorite structure with no evidence for ordering of oxygen vacancies. Particles with composition close to 50% Ce may show excellent activity or very poor activity depending on their structure. The less active nanoparticles have a predominant pyrochlore-type structure with cation ordering. The presence of the reduced phases can be used to explain the decreased reduction percentages after high temperature redox treatment.

Acknowledgment. This work was supported by the National Science Foundation through grant NSF-CTS-0306688. We acknowledge the use of TEM facilities at the John M. Cowley Center for High Resolution Electron Microscopy at Arizona State University.

References

(1) Trovarelli, A. *Catal. Rev.—Sci. Eng.* **1996**, *38*, 439.
(2) Fornasiero, P.; Balducci, G.; DiMonte, R.; Kaspar, J.; Sergo, V.; Gubitosa, G.; Ferrero, A.; Graziani, M. *J. Catal.* **1996**, *164*, 173.
(3) Kaspar, J.; Fornasiero, P.; Graziani, M. *Catal. Today* **1999**, *50*, 285.
(4) Di Monte, R.; Kaspar, J. *J. Mater. Chem.* **2005**, *15*, 633.
(5) Park, S. D.; Vohs, J. M.; Gorte, R. J. *Nature* **2000**, *404*, 265.
(6) Mogensen, M.; Sammes, N. M.; Tompsett, G. A. *Solid State Ionics* **2000**, *129*, 63.
(7) Wang, R. G.; Crozier, P. A.; Sharma, R.; Adams, J. B. *J. Phys. Chem. B* **2006**, *110*, 18278.
(8) Fally, F.; Perrichon, V.; Vidal, H.; Kaspar, J.; Blanco, G.; Pintado, J. M.; Bernal, S.; Colon, G.; Daturi, M.; Lavalley, J. C. *Catal. Today* **2000**, *59*, 373.
(9) Liotta, L. F.; Macaluso, A.; Longo, A.; Pantaleo, G.; Martorana, A.; Deganello, G. *Appl. Catal., A* **2003**, *240*, 295.
(10) Baker, R. T.; Bernal, S; Blanco, G.; Cordon, A. M.; Pintado, J. M.; Rodriguez-Izquierdo, J. M.; Fally, F.; Perrichon, V. *Chem. Commun.* **1999**, *2*, 149.
(11) Montini, T.; Hickey, N.; Fornasiero, P.; Graziani, M.; Banares, M. A.; Martinez-Huerta, M. V.; Alessandri, I.; Depero, L. E. *Chem. Mater.* **2005**, *17*, 1157.
(12) Wang, R. G.; Crozier, P. A.; Sharma, R.; Adams, J. B. *Microsc. Microanal.* **2006**, *12* (Suppl 2), 770.
(13) Sharma, R.; Crozier, P. A.; Kang, Z. C.; Eyring, L. *Philos. Mag.* **2004**, *84*, 2731.
(14) Vidal, H.; Bernal, S.; Kaspar, J.; Pijolat, M.; Perrichon, V.; Blanco, G.; Pintado, J. M.; Baker, R. T.; Colon, G.; Fally, F. *Catal. Today* **1999**, *54*, 93.
(15) Kang, Z. C. *J. Alloys Compd.* **2006**, *408*, 1103.
(16) Perez-Omil, J. A.; Bernal, S.; Calvino, J. J.; Hernandez, J. C.; Mira, C.; Rodriguez-Luque, M. P.; Erni, R.; Browning, N. D. *Chem. Mater.* **2005**, *17*, 4282.

NL073135C